Preprint Title Thickness Dependent Oxidation in $CrCl_3$: a Scanning X-ray Photoemission and Kelvin Probe Microscopies Study

Authors Shafaq Kazim, Rahul Parmar, Maryam Azizinia, Matteo Amati, Muhammad Rauf, Andrea Di cicco, Seyed J. Rezvani, Dario Mastrippolito, Luca Ottaviano, Tomasz Klimczuk, Luca Gregoratti and Roberto Gunnella

Publication Date 03 Feb. 2025

Article Type Full Research Paper

Supporting Information File 1 SI_Beilstein Journal of nanotechnology.zip; 2.6 MB

ORCID® iDs Shafaq Kazim - https://orcid.org/0000-0001-6288-7354; Maryam Azizinia - https://orcid.org/0000-0003-2483-5806; Dario Mastrippolito - https://orcid.org/0000-0001-6360-7254; Roberto Gunnella - https://orcid.org/0000-0003-4739-6375

Thickness Dependent Oxidation in $CrCl_3$: a Scanning X-ray Photoemission and Kelvin Probe Microscopies Study

S. Kazim[1], R. Parmar[2], M. Azizinia[1], M. Amati[2], M. Rauf[1], A. Di Cicco[1], S. J. Rezvani[1], D. Mastrippolito[3], L. Ottaviano[3,4], T. Klimczuk[5], L. Gregoratti[2] and R. Gunnella[*1]

Address: [1]Physics Division, School of Science and Technology, University of Camerino, 62032 Camerino (MC), Italy; [2]Elettra-Sincrotrone Trieste, Strada Statale 14, AREA Science Park, 34149 Trieste, Italy; [3]Dipartimento di Scienze Fisiche e Chimiche (DSFC) Università degli Studi dell'Aquila, Via Vetoio 10 67100 L'Aquila, Italy; [4]CNR-SPIN UoS L'Aquila. Via Vetoio 10 67100 L'Aquila, Italy and [5]Gdansk University of Technology, Faculty of Applied Physics and Mathematics, 80-233 Gdansk, Poland

Email: R. Gunnella - roberto.gunnella@unicam.it

[*] Corresponding author

Abstract

The modifications in the electronic properties induced by the thickness and size of an individual flake of transition-metal halides on different substrates (Si oxide or In-doped tin oxide) are of particular technological interest and even more in the case of the chromium trihalide, whose longer lifetime in ambient conditions is particularly intriguing. By employing synchrotron-based Scanning Photoelectron Microscopy (SPEM) with 0.1 μm resolution and Kelvin Probe Force Microscopy (KPFM), and evaluating the surface modification reaction and surface potential, we established the correlations of the two latter properties with the thickness of flakes, observing a natural tendency to preserve their characteristic when the flakes have significantly less thickness. This preliminary study investigates interfaces made by dry transfer of $CrCl_3$ flakes, which induce spin-orbit coupling to systems, otherwise lacking this property.

Keywords

Two-dimensional material; Mechanical Exfoliation; CrX_3; Kelvin Force Microscopy; Scanning Photoelectron Microscopy (SPEM); Chemical Mapping; work function

Introduction

The family of chromium-based trihalides has garnered significant interest in recent years, particularly after the fascinating discovery of long-lasting magnetism in a single layer of CrI_3 [1]. In our previous reports, we dealt with the environmental stability of $CrCl_3$, which can be easily exfoliated while exhibiting a lower degradation rate than other CrX_3 (X = I or Br) [2,3]. To maximize the potential of any material, a detailed understanding of its electronic and structural changes resulting from intrinsic and extrinsic defects is necessary [4]. It should be noted that little experimental research has been conducted on the electronic structure of CrX_3 [5,6]. In accordance with previously published photoelectron spectroscopy results, CrX_3 belongs to metal compounds where the 3d states are very close to the Fermi level, well above the 3p/4p/5p states of the halides and this was confirmed by Antoci and Mihich [7] through the self consistent band structure calculations. In these calculations, spin degeneracy was introduced, resulting in $CrCl_3$ and $CrBr_3$ behaving as metallic system confirming the influence of 3d states on the Fermi level. In our previous publication,[8-10] we have found the formation of a stable and partially ordered Cr-O-Cl surface on a vacuum-or air- cleaved samples of $CrCl_3$. Here, we aim at extending the chemical and structural analysis following our previous results from electronic and optical properties of mechanically cleaved $CrCl_3$ samples [2,8,10,11], focusing to thin layer flakes and their dependence on the layers thickness, obtained by spectro- and scanning- microscopy with the lateral resolution of a few tens of nanometers. If an aspect not to neglect is the interface with the supporting substrate, [3,12] more important thing is the quantification of the properties of flakes that can be significantly different from those of the bulk [1,13]. One central problem is also whether the modified structure and chemical stoichiometry with respect to the bulk is caused by the stress applied during cleaving, affecting the surface terminations that would be found on cleaved crystals [10] and if similar effects

are generated during the exfoliation, that is relatively different with respect to the cleaving process. In bulk, we demonstrated that cleaved surfaces by oxygen adsorption allow formation of a stable structure with charge transfer signatures that we addressed by high resolution photoemission[8]; would it be different on thin exfoliated flakes ? Like in other materials, the content of defects such as ad-atoms, grain boundaries length, vacancies and substitution impurities influences the electrical, magnetic and electronic properties of the final device [4,14,15]. To name one , the formation of chalcogenide vacancies is often related to the enhanced dissociation of molecular oxygen [16] at the metal species. These defects do not only change the electronic behaviour of the sample by modifying the band structure [17] but are also responsible of Curie temperature deviations, work function modification [18] and induced long-range magnetic orders (i.e., magnetic band effect) [19-21]. A well known and suitable technique to investigate the electronic structure on surfaces is the X-ray photoemission spectro-microscopy [6,22]; in order to assume the necessary spatial resolution the beam size must be reduced to tens of nanometers. The ESCA Microscopy beamline [23] performs this task by means of a zone plate arrangement that can reduce the beam size to 130 nm in diameter and its grazing collection angle can provide a highly surface sensitive probing depth of approximately 1 nm [23,24]. Such a short mean free path condition could be suitable for increasing sensitivity to a number of defects per unit volume, forming at the surface, that can be recorded by the significant photoemission core level binding energy shift[25,26]. The significance of these studies lies in the exploration of novel materials with improved properties for 2D magnets by manipulating factors such as layer thickness, applied strain, and induced defect sites. Numerous theoretical studies predict that magnetic order in monolayers occurs at temperatures significantly higher than the bulk Curie temperature (i.e. 17 K). In their work, Liu et al. employed Monte Carlo methods to observe ferromagnetic behaviour in monolayers below 66 K and proposed that hole doping could further enhance the Curie temperature [21]. Similarly, another Monte Carlo study found that the transition temperature for monolayer $CrCl_3$ is 49 K, proposing that the Curie temperature could be further increased by applying uniaxial strain [17] [27].

In the present study, we examined the surface modifications that occur in thin layers of exfoliated

$CrCl_3$ (approximately 1 to 20 ML) by using scanning photoelectron microscopy (SPEM). We have collected the chemical maps and spectra of the Cl and Cr core levels at room temperature (RT) and at 300°C temperature. By monitoring the core levels and valence band spectra at various spatial resolutions ($\geq 0.13\mu m$), we obtained quantitative maps of the chemical composition to correlate these maps with the thicknesses measured by AFM. Additionally, we investigated the correlation between the microscopic results and the surface potential of $CrCl_3$ flakes at the nanoscale level using Kelvin probe microscopy [28]. Kelvin Probe force microscopy (KPFM) was primarily used to measure the local contact potential difference between the conducting AFM tips and the sample, and enables high-resolution mapping of the work function and surface atomic states [29]. By doing so, this technique helps to provide a correlation between the valence band photoemission information and the morphological information and provides insights into the position of the conduction band [30].

Results and discussion

Optical contrast and AFM

It is well known that 270 nm thick SiO_2/Si substrates provide the highest optical contrast value for a single or few layers of $CrCl_3$ [2,11]. Due to the insulating behaviour of 270 nm Si substrate and to avoid surface charging, we used as substrates Si(001) wafers with 1 nm native SiO_2 and ITO films (190 nm) on glass substrates. On the native Si substrates, the optical contrast was too low to make thin flakes visible. We had the limitation that we could not visualize flakes with thicknesses less than 10 nm by the optical microscope (the lowest visible contrast on these substrate). Fig.1 gives a direct comparison of AFM images and optical contrast on the 1 nm SiO_2/ Si substrate. Reporting at the same time the optical contrast, the AFM image and an entire series of profiles showing the layer thicknesses. On the ITO substrate, we systematically performed the optical and AFM measurements and reported the comparison in Fig.2(a,b). Based on the colours of the flakes seen in the optical microscope images, an interval of thickness values of each flake could be determined. Since we have already mentioned that flakes less than 10 nm thick on 1 nm SiO_2/Si substrates are

hardly visible, we have defined the colour range starting from 10 nm or higher. On SiO_2 in Fig.1 light olive color corresponds to the range 10 nm to 20 nm, brown colour corresponds to 20 nm to 40 nm, blue corresponds to 40 nm to 80 nm, and yellow represents flakes between 80 nm to 120 nm thickness. Similarly, on ITO substrate, but with higher sensitivity, the colours are defined in SM as shown in Fig.SM1.

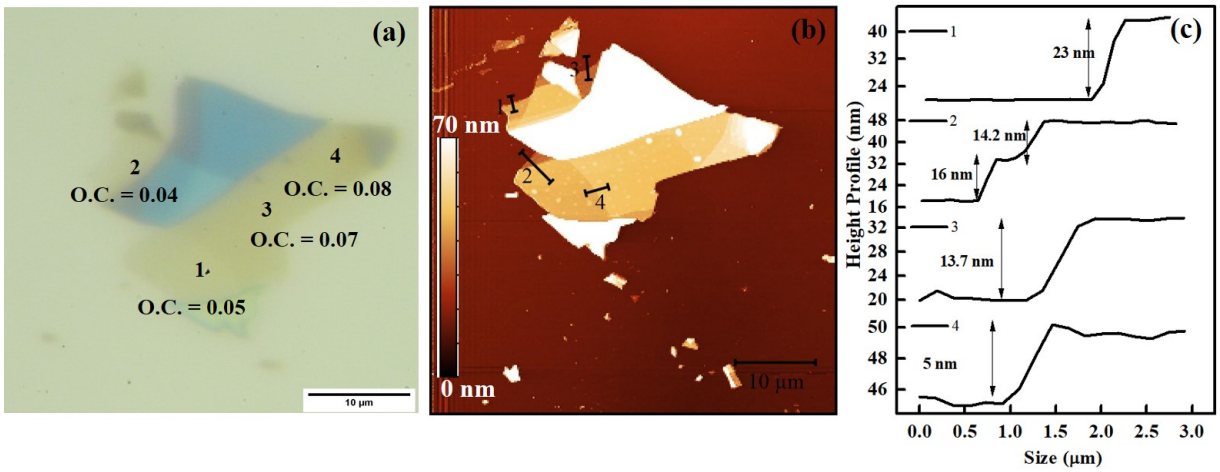

Figure 1: Optical contrast (a) and morphological characteristics (b) of mechanically exfoliated $CrCl_3$ flakes on the native Si (1 nm SiO_2) substrate. The plots in panel (c) are representing the thickness profile scans through the various flakes as denoted in Fig.1b.

In the latter case we distinguished the lean (L) and thick (T) flake by optical and AFM inspection. The Olympus B×60 system with objective lenses of 5×, 10×, 20×, 50×, and 100× magnifications was set in order to find a color scale to interpolate with AFM thickness measurement results. In Fig.1-(a) and Fig. 2-(a), we reported a series of $CrCl_3$ flakes of different thicknesses on Si and ITO substrates based on optical determination and in Fig2-(b) and Fig3-(c), the related AFM images to evaluate the thickness. It is evident that profile 3 in Fig.1 (b) shows the minimum observable flake of $CrCl_3$ from the substrate, in Fig.1 (a). On the other hand, in Fig. 2-(a) clear microscopy images of a few layers of flakes were shown. According to the optical contrast value, L and T represent the lean and thick step, respectively. The negative value of optical contrast shows that the surface of $CrCl_3$ looks brighter than the substrate. We have shown this thickness variation by AFM micrographs on the specific zoomed regions in Fig. 2 (e) and (f) where the height of profiles (T and L) were taken.

Spatially resolved Photoemission

We studied the layer-dependent surface modification of $CrCl_3$ by SPEM, one of the optimal experimental techniques (Fig.11) for this kind of study. The use of the zone plate and order selection aperture (OSA) provides an ideal spot size for the study of 2D materials, focusing on the character of the material in relation to its shape. In fact, sample flakes in the range of 1-10μm^2, obtained by the exfoliation technique, can be analysed by the SPEM microscope on such a characteristic length by the precise control of the relative position between the beam and the sample, to get a determination of predominant phases immune from inhomogeneities and spurious effects, like zone at the boundary of the flakes, or with different thickness. Furthermore, the overwhelming background arising from the substrate can be minimized by the special design of the detection system[23]. In SPEM, the spectra can be recorded by arrangements in three mode conditions: 1) focused (beam size$\sim$ 130 nm); unfocused beam ($\sim$2 μm); the so called OSA mode ($\sim$ 75 μm).

Fig. 3 presents the survey spectra with all three aforementioned conditions on thin $CrCl_3$ flakes at RT on a native Si oxide substrate. These survey spectra evidenced the beam damage due to a focused beam, represented by the high intensity of Si 2p core level photoemission, not shown in the other cases like the defocused beam experiments. A different situation is the OSA measurement spectrum which displayed the Si component because of the wide beam diameter. This conclusion is also confirmed by the evaluation of the $CrCl_3$ stoichiometry in the last two cases.

Table 1: Atomic element contributions under different incident photon beam size.

Stoichiometry composition through survey spectra.			
Used Beam description	Cl 2p area	Cr 2p area	Cl/Cr ratio
Focused Beam	2190	4430	0.69
Defocused Beam	7500	5050	2.1
OSA Beam	24900	11500	3.0

The table 1 represents the area under the peak for Cl 2p and Cr 2p; the stoichiometry was obtained after the correction with sensitivity factor as reported in the SI. The stoichiometry of $CrCl_3$ is found to be consistent with the nominal one in OSA beam conditions but was found significantly deviating when obtained with smaller size beam, with the thin specimens being under high photon

dose for several minutes. Such a behavior is confirmed by the signal from Si 2p core level of the underlying substrate. On the contrary in the case of OSA mode, the contribution from the substrate is expected because of the extended beam size. While capturing the maps, the sample was scanned continuously and the recorded point of map was taken within few milliseconds, which drastically reduced the incident photon dose compared to survey spectra. The drawback is the lower statistical quality of the spectra.

In Fig. 4, we have selected one particular flake which consists of two main different regions on the SiO_2 (1nm)/ Si substrate. Fig. 4(a) shows the Cl 2p map after background correction at a binding energy of about 200 ± 4 eV. We know from a previous work that at this energy Cl 2p core level only shows the main component at 199.5 eV. [8]. On the contrary in Fig. 4(c) the Cr $2p_{3/2}$ shows also a second component at 576 eV in addition to a 577.5 eV main one. Both maps display an increased intensity from Cl emission from the parts on the right with respect to the thicker one on the left where the Cl vacancies density is supposedly higher (see inset of Fig.4-(a)). In some recent works, the signature of the formation of a Cr-O-Cl surface phase [8,10] was characterized by the presence of a low binding energy component for Cl 2p at 198 eV (Fig.4-(b)) but for high degree of oxidation at high temperature in ambient air that we do not observe here, and a low binding energy component for the Cr $2p_{3/2}$ at 576 eV ((Fig.4-(d)) appearing from the first stages of presence of oxygen also in UHV. Such a deviation and component appearance is clearly visible on the thicker region of the sample (left region) for the Cr 2p core level. Locally the component is also enhanced in case of portion of surface where the beam effects have been important (light blue square in Fig.4-(c)) but it is almost absent elsewhere.

After the AFM study, we performed the core level analysis on the ITO substrate. Fig. 5 (a) shows the Cl 2p map around 199.5 eV binding energy, where we located the leaner and thicker regions as point L and point T respectively. Fig. 5 (b) shows the Cl 2p spectra taken from the respective coloured region after background correction. The upper panel spectrum was taken from point L and lower panel spectrum from point T. The same Cr $2p_{3/2}$ map was reported in Fig. 5 (c), and the corresponding Cr $2p_{3/2}$ core level data were shown in Fig. 5 (d). The data were shifted vertically

for better visualization. From the Cr 2p spectra, one can clearly see the fingerprint of the low binding energy component for the thick sample, which is clearly absent in the thinner part (L). From our previous report, we know that the low-binding energy component emerges after the formation of O-$CrCl_3$ phase.[8].

To confirm our analysis, we have continued the investigation through the Cr 2p 3/2 and O 1s core level spectra in Fig.6 at different thicknesses on ITO substrate as reported in Fig. 2 with defocused beam and observed a fine appearance of the peak at the lower binding energy of Cr 2p for the thick region, while the O 1s spectra appear to be enhanced for the same region.

This result has the merit to complement the study on cleaved samples [8], where the formation of a stable phase by help of oxygen in interstitial position of the surface, was providing a redox source for the Cr atoms, showing the formation of a low binding energy component Cr 2p core level.

Here, the evidence that this process might occur only in presence of defects (Cl vacancies) and in the case of the thicker flakes, makes us conclude that one of the reason of the resilience of the $CrCl_3$ flakes is that the formation of Cr-O-Cl phase must be triggered by a sufficient volume of material,i.e., that the origin of the oxygen driven phase formation is hindered if there is no availability for specific diffusion processes in the samples.

All three SPEM figures Fig.4, 5 and 6 confirm that a lower binding energy component at 576 eV appeared due to the presence of Cl vacancies and subsequent formation of reactive sites of dissociation [16] of molecular oxygen to induce a stable phase of Cr-O-Cl. [8].

We realized that the low binding energy component in Cr $2p_{3/2}$ is arising due to the charge transfer effects turning the system from a surface Mott-Hubbard insulator to a charge-transfer[8] ones in spite of Cr being an early transition metal [31].

What can be presumed from the present study is that Cl-O exchange following Cl vacancy formation is limited in very thin layers because of the limited diffusion process and the lower number of defects present per unit volume that can be exploited in the process. These numbers are incremented by the beam power, when damages occurs as shown through light blue area in Fig. 4 .

These results are consistent with previous studies on bulk samples, which were cleaved in vacuum, where such a formation was very much hindered with respect to thick flakes prepared in air. [8] It is nevertheless important to stress that here the modification is driven by the Cl vacancy alone for the most. And a strong evidence from this and previous studies [8] is that only in case of air cleavage of bulk samples we observe the huge Cl vacancy signatures in Cl 2p core levels by a low energy component at 198 eV. Our conclusion is that the thin $CrCl_3$ layers are more difficult to be modified because of the high energy of defect formation and the rapid quenching of them by mobile free atoms, and this is confirmed by the high energy of Cl vacancies found by total energy calculations [9].

Kelvin probe force microscopy (KFM) measurements

One look at the surface potential of the samples could complement our analysis. Fig.7 (a) and (c), reveal the topographic maps and their corresponding thickness profiles of $CrCl_3$ flakes on SiO_2 substrate. The average thickness of L and T $CrCl_3$ flakes on SiO_2 substrate is about 5.3 nm and 76.5 nm, respectively. While Fig.7 (b) and (d) show the Kelvin potential map and the corresponding potential profiles. An obvious variation in flakes Kelvin potential (V_{KP}) , the difference between the surface potential of tip and samples, with respect to the substrate could be observed, which is associated with their work function difference. In the V_{KP} line profiles, the flat region (at high potential) corresponds to the substrate, while the downward curved region (at low potential) is related to flakes. The V_{KP} of L and T flakes are 0.1 V and 0.04 V, respectively. Based on the V_{KP} values, the work function of L and T flakes is about 5.4 eV and 5.46 eV, respectively, considering the work function of Pt tip is 5.5 eV. As a control check the work function of SiO_2 results to have the correct value of 5.0 eV.

To complete the work done by the spatial resolved photoemission on the ITO substrate, for the obvious reasons related to the better conductive character, and a better contrast in the process to individuate the flakes, we analyzed flakes as in Fig.8 in which the thickness is plotted as a function of the position on the analyzed line. The flake L has a work function of 5.39 eV (thickness 6.6 nm)

and 5.43 eV for T (14 nm thickness), while 5.34 eV is the value for the substrate (ITO level). From the analysis of the surface potential on $CrCl_3$ flakes represented in Fig.8, it can be seen that also in this case the areas with larger thickness have higher surface potential and are more close to the tip surface potential.

In both substrates, the KFM results of flakes show a similar behavior i.e., the flake T has a higher work function as compared to the flake L.

This variation in the work functions of flake is attributed to the chlorine vacancies in the thick region which promote the chemisorption of oxygen and act as charge acceptor [32], but in less efficient way with respect to the Cl, as we observed by the low binding energy peak in Cr 2p SPEM spectra. On the contrary to physisorption, the chemisorption of oxygen possesses a significant impact on the electronic properties of a material. Neal *et al.* [33] reported the effect of chemisorption oxygen as a p-type doping, which shows consistency with our results.

We expect the surface potential accompanying the same behavior of the evolution found on the chemical composition by the spatial resolved photoemission [34].

Valence Band results

The valence band spectra of $CrCl_3$ flakes were recorded at two different regions, i.e., T and L. Fig.9 shows the valence band maxima (VBM) for both regions. The VBM at point L is about 1.82 V while at the point T the foot of the VB is at 1.74 V, indicating the difference of 0.08 V which is significantly above the limit of the experimental resolution. These VBM results of both regions reveals that, point T is closer to the Fermi level as compared to the point L. This modulation of Fermi level is primarily attributed to the existence of Cr-O-Cl phase in the thick region. As reported in the KFM results, the work function of point T is higher as compared to point L. The difference in the work function of these points in the KFM results is about 0.06 V, which is consistent with the VBM results.

Discussion and conclusions

Our work is aiming at providing the control of the surface evolution of thin specimens of $CrCl_3$, contributing to establishing the method to engineer the material. In this specific case, It is hard to know the real reason of the composition modulation we have observed through the spatial resolved techniques, but it could be the result of the combined effect of vacancies and possible induced dissociation of molecular oxygen. KFM can be an interesting tool to describe the variation of chemical character of the 2D flakes with sizeable details. In Fig.10 we report the $CrCl_3$ values of surface potential measured in different conditions on flakes of various thicknesses on SiO_2 and ITO substrates. As it can be seen a steep increase of the surface potential represents the most evident variation on the $CrCl_3$ surface, where a higher surface potential is related to a higher level of oxidation of the thicker flakes probably related to increase of Cl vacancies density acting as dissociation centers and formation of a Cl defective or O/$CrCl_3$ surface structure [10,35] Similarly to what highlighted by the SPEM measurements, being both studies surface sensitive, the counter-intuitive finding of lower degree of oxygen contamination is self corroborating the conclusion of this behavior as general trend for this material, being an aspect of particular relevance because of the possible applications to monolayer thin devices.

Experimental details

Preparation of exfoliated $CrCl_3$ flakes from the single crystal bulk material was reported in our previous papers [2,11]. Though preferentially a 270 nm silicon oxide substrate would help the determination of flakes thickness, we used also more conductive substrates to measure photoemission under the X-ray beam, i.e., 1 nm thick native oxide Si substrates. Another convenient substrate for SPEM was the 190 nm thickness of indium-doped tin oxide (ITO), guaranteeing the necessary conductivity during the photoemission process. The 190 nm thickness was also important during the process of optical selection by showing significant contrast at the optical microscope ($\times$ 50 magnification), helping a better localization of thin flakes. The SPEM measurements were performed at ESCA Microscopy beamline 2.2L in Elettra Synchrotron Trieste facility, Italy. The incident photon

energy of ~ 740 eV was calibrated by means of Au $f_{7/2}$ at 84.0 eV from a clean gold foil sample. To reduce the beam induced effects on the samples, we took the high energy resolved spectra with an unfocused beam (~ 2.0 μm diameter), while the high-resolution SPEM maps of 128×128 μm^2 size using a piezoelectric driven stage, were obtained with focused beam (pixel size of 130 nm) by means of a Fresnel zone and a relatively broad energy resolution mode [23] . The SPEM maps were captured through a 48 multi-channel delay line detector.

To analyze the photoelectron intensity of an individual atomic element on the captured SPEM maps, the image was subjected to background correction by eliminating the topographic features. We also applied the (3×3) filter to reduce the noise before extracting the photoemission spectra from the particular SPEM map. Fig.11 shows the schematic setup of the focusing optics and the hemispherical photoelectrons detector arrangement of the SPEM system.

Atomic Force Microscopy (AFM) images were acquired with the NanoObserver (CSI) AFM system in resonant mode using an n-type Si cantilever coated with Pt at resonance frequency of 68 kHz with elastic constant of 1-5 N/m (AppNano) and doped diamond tips with 120 kHz and 8 N/m elastic constant (ADAMA). Kelvin probe force microscopic (KPFM) images were taken by the double passage before and after applying the electric field by elevating the tip about 50 - 150 nm to measure the surface potential and avoid the morphological features. The applied voltage was varied from 0.2 to 1 V without significant changes in the surface potential value recorded. All micrographs were recorded at room temperature.

Acknowledgements

The authors acknowledge that the results presented in this paper were initially discussed at the Società Italiana Luce di Sincrotrone meetings 2021 and at the IEEE Nanotechnology Materials and Devices Conference (NMDC) in 2023 through poster and oral presentations, respectively. Furthermore, we refer to the abstract published as part of the conference proceedings: doi = 10.1109/NMDC57951.2023.10344256

Funding

This work has been funded by the European Union - NextGenerationEU under the Italian Ministry

of University and Research (MUR) National Innovation Ecosystem grant ECS00000041 - VITALITY - Spoke 9 and the PNNR MUR Project PE0000023 NQSTI.

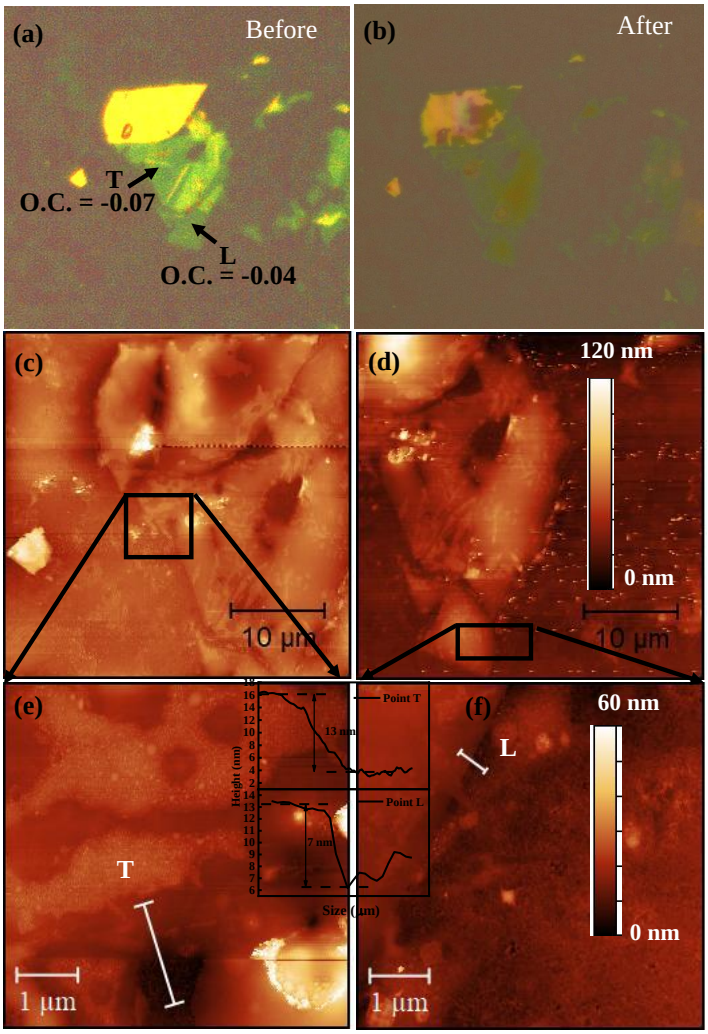

Figure 2: Optical contrast on ITO substrates before (a) and after (b) the SPEM measurements. Morphological characteristic of $CrCl_3$ on ITO substrate for the T and L points in panel (a), reported respectively in (c) and (d), together with their zoomed details in (e) and (f). In the inset are shown the thickness profile of T and L respectively.

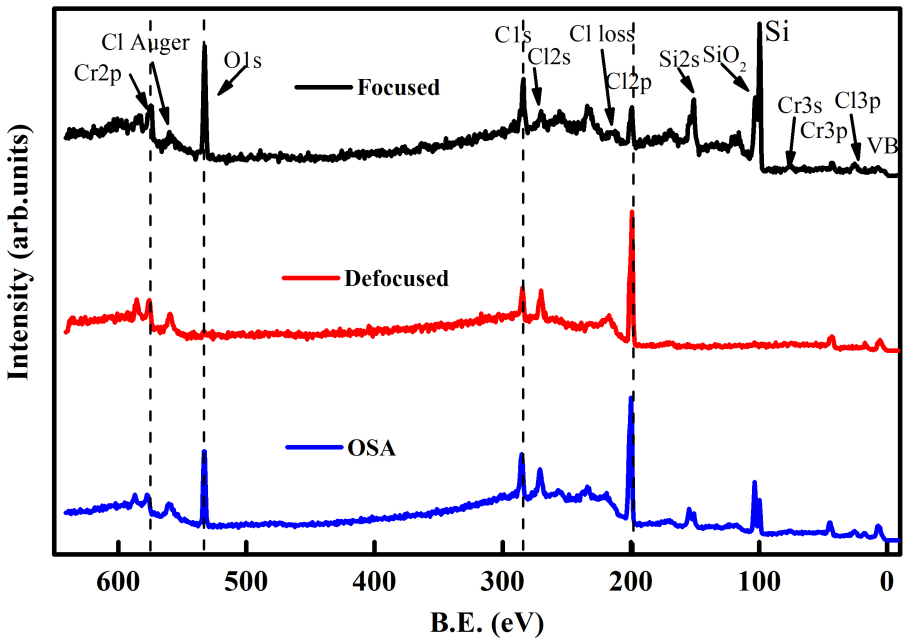

Figure 3: Survey spectra on exfoliated $CrCl_3$ flakes on native Si oxide substrate with different beam conditions at RT. From the top focused , defocused and OSA modes of operation respectively.

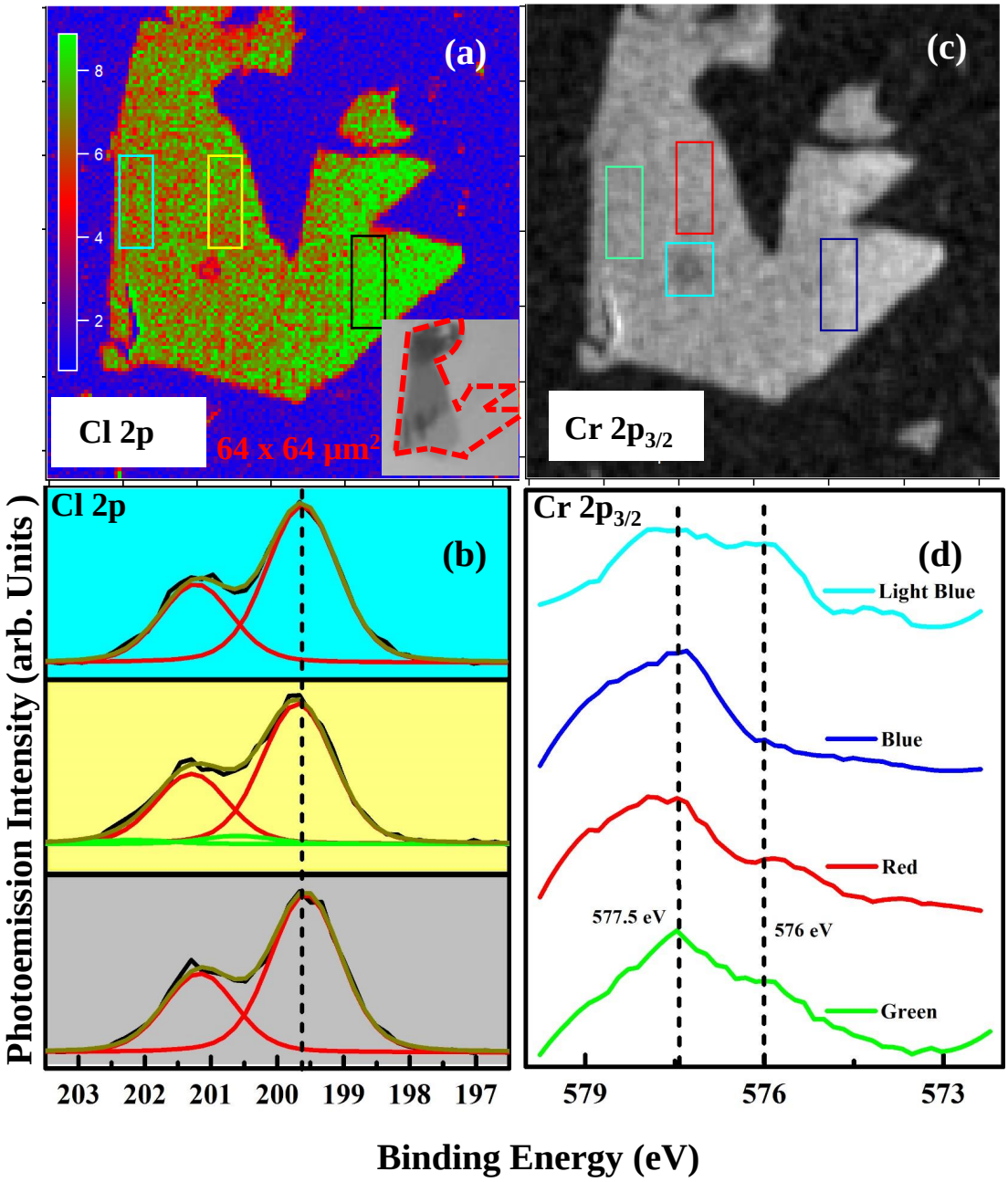

Figure 4: Cl 2p and Cr $2p_{3/2}$ core level SPEM maps with focused beam at RT on 1 nm SiO_2/ Si substrate:(a) Cl 2p map at 199.5 eV binding energy; (b) Light blue, yellow and black stacked spectra were taken from corresponding color rectangle areas (c) Cr $2p_{3/2}$ map at 577.5 eV binding energy (d). The binding energy spectra acquired from respective colored areas.

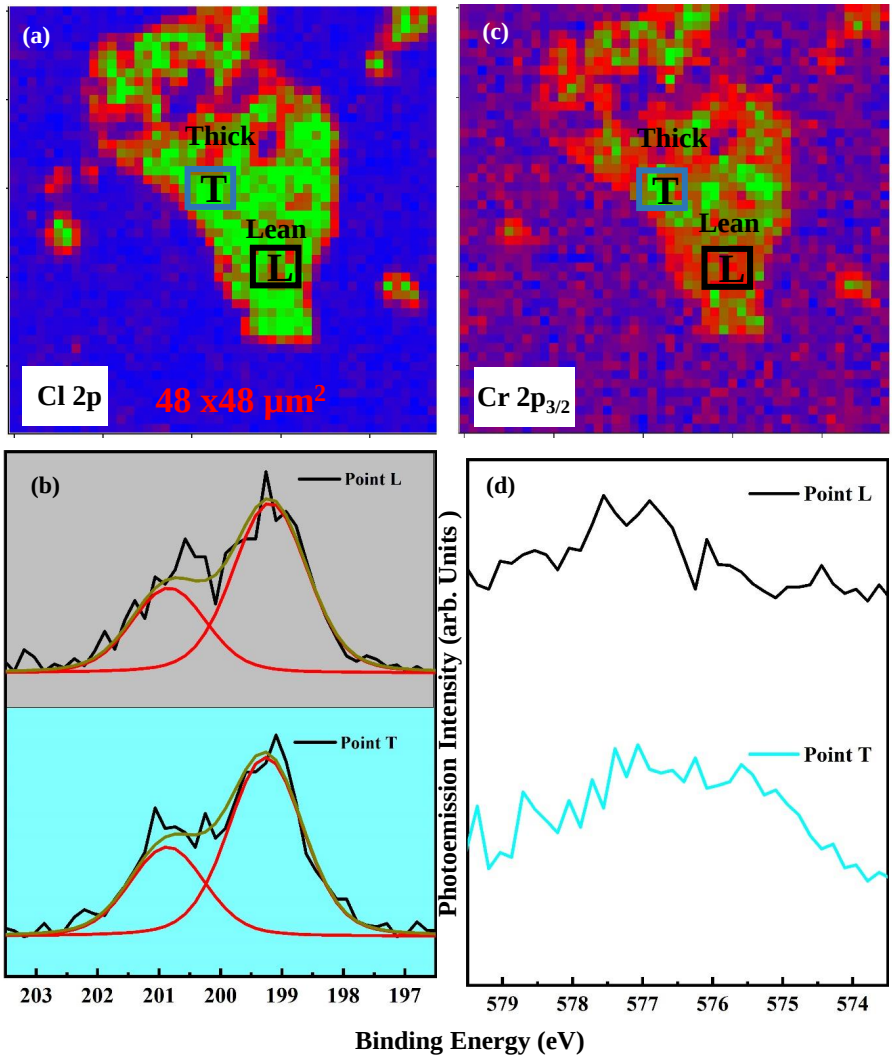

Figure 5: Cl 2p-(a,b) (map and spectrum) and Cr $2p_{3/2}$ core level maps about 200 eV and 576 eV binding energies respectively.

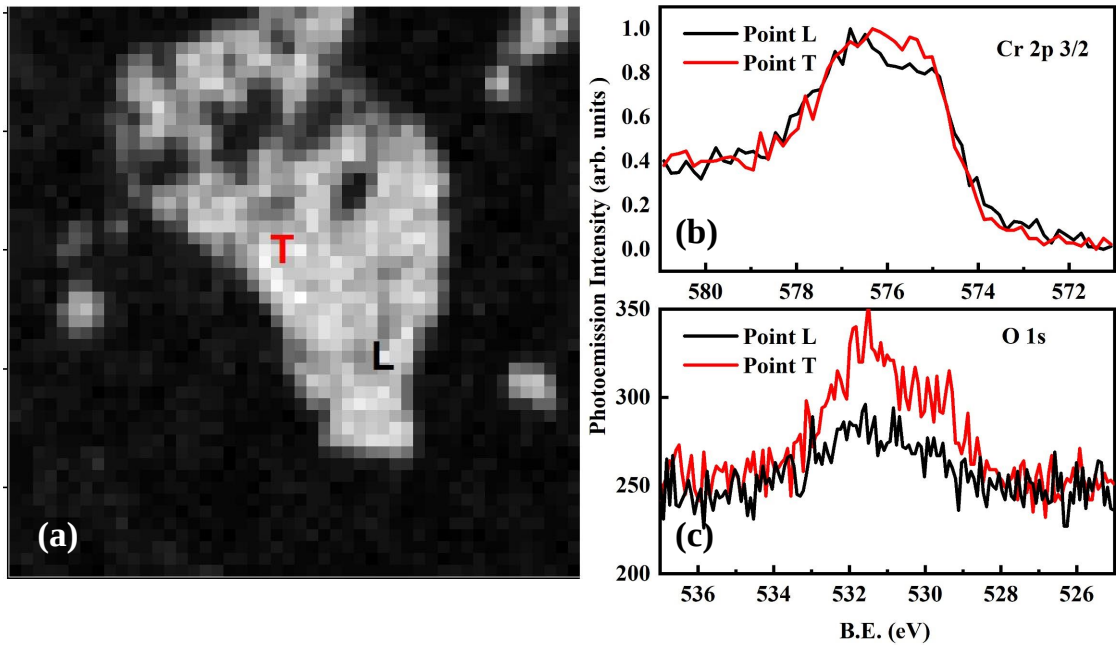

Figure 6: SPEM spectra from thick (T) and lean (L) areas : (a) SPEM image to verify the area of interest. (b) Cr $2p_{3/2}$ core level spectra (c). O 1s core level spectra substrate used is ITO.

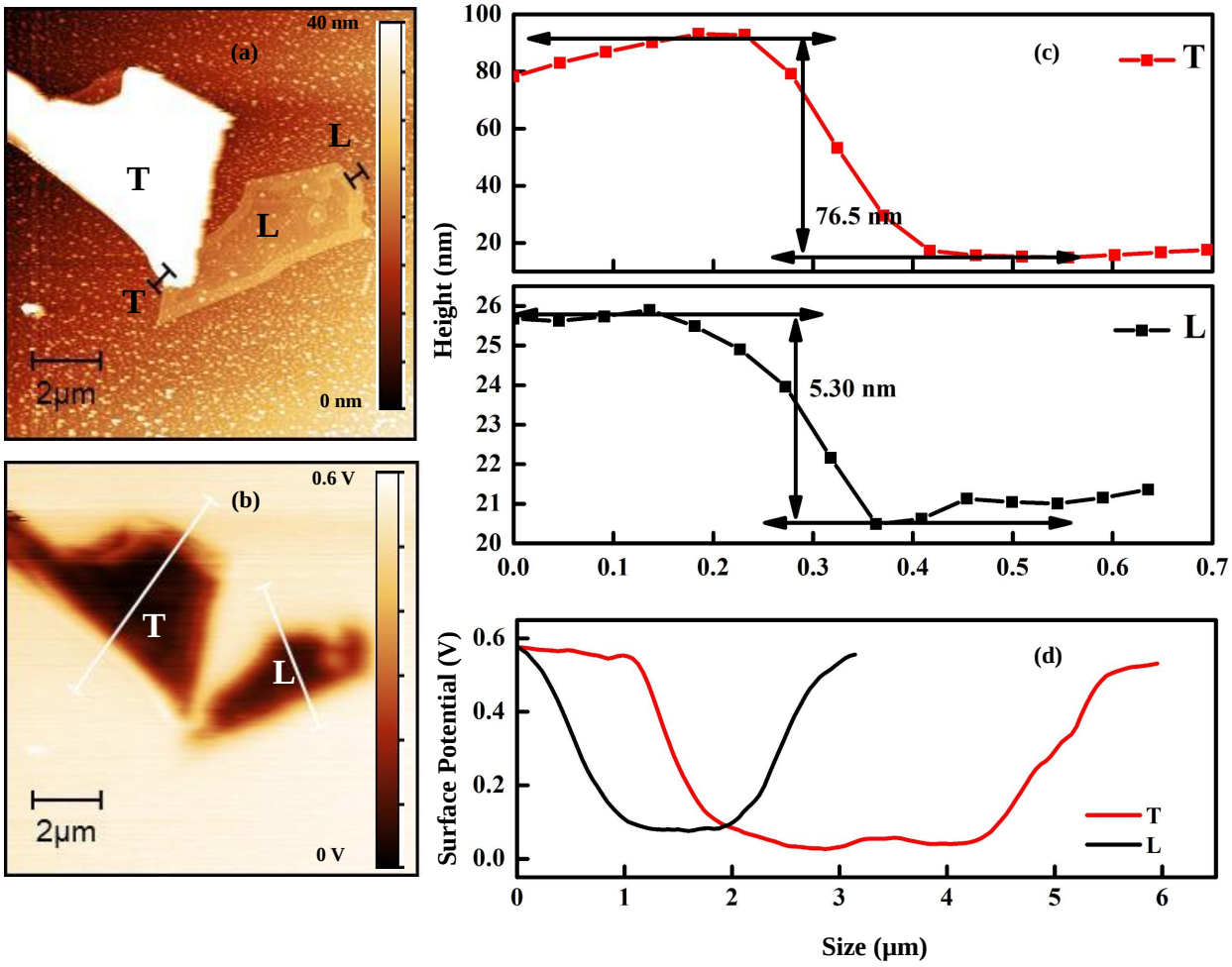

Figure 7: $CrCl_3$ on SiO_2/Si substrate: a) topography by non-contact mode AFM of two different thickness flakes; b) Kelvin surface potential of the samples on SiO_2; c) z-profiles of the two flakes; d) Kelvin surface potential scans along the profiles of a). Pt tip was used.

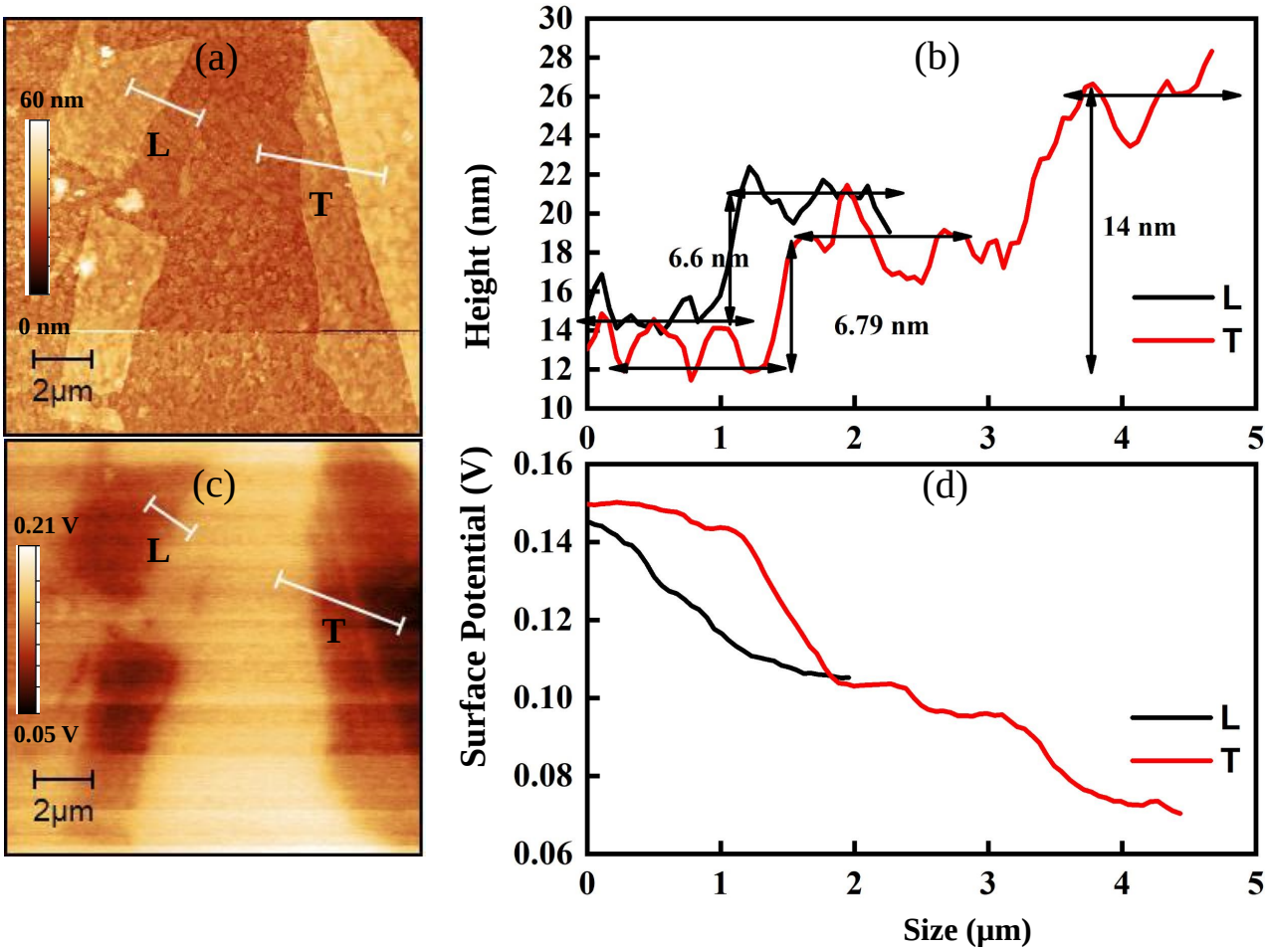

Figure 8: a) Topography by non-contact mode AFM of two different thickness flakes deposited on ITO; b) Kelvin net surface potential of the samples in a); c) z-profile of the two flakes; d) Kelvin surface potential scans along the profiles of a). Measurements tip is Pt coated.

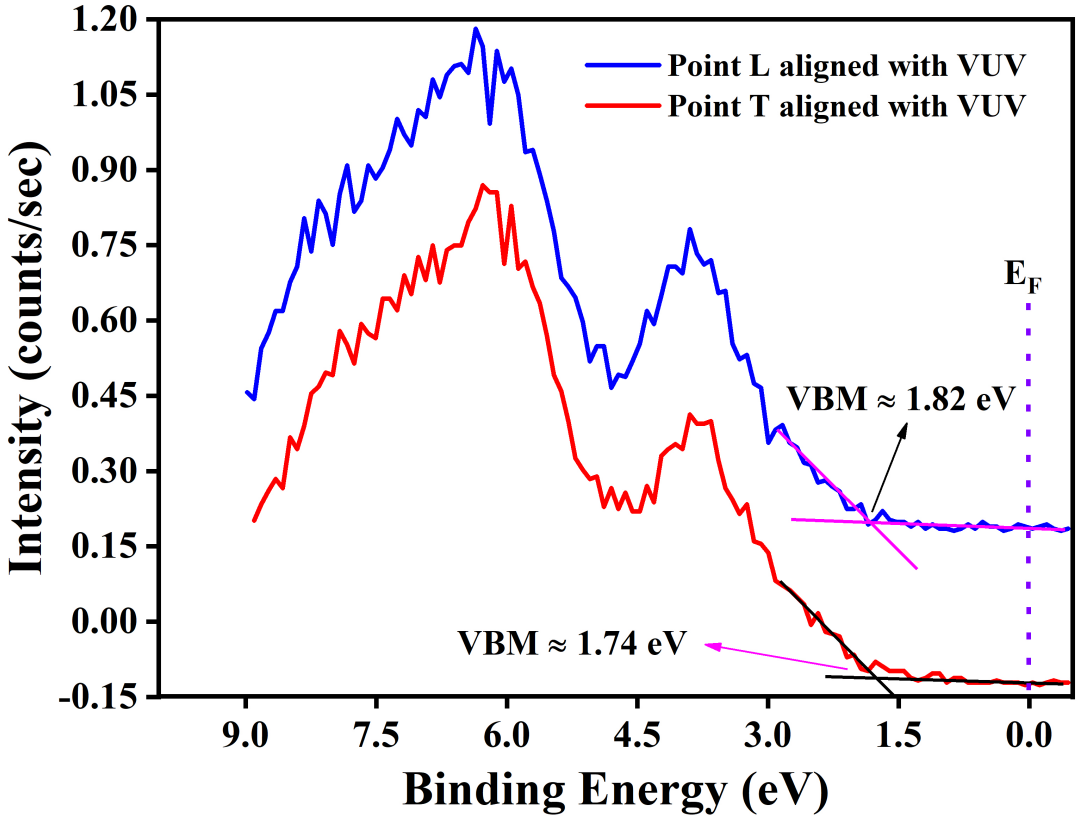

Figure 9: Valence band spectra acquired at point L and point T (thick). The spectra were aligned with respect to our previously published high resolution photo-emission spectra at 130 eV photon energy[8]. The alignment is shown in SM fig 3.

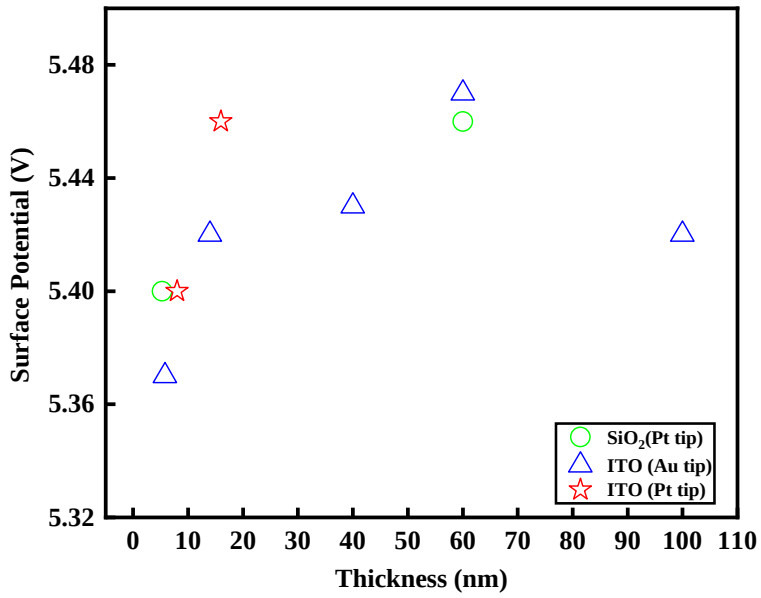

Figure 10: The values assumed by the surface potential of $CrCl_3$ flakes after several experiments vs their thickness as determined by AFM. In Green the points taken on SiO_2 substrate 285 nm on Si by the Pt tip (kelvin potential 5.5 eV) in red the potential taken by Pt tip on ITO substrate (190 nm) on glass; in blue the surface potential taken by the Au tip (5.1 V) on ITO substrate (190 nm) on glass.

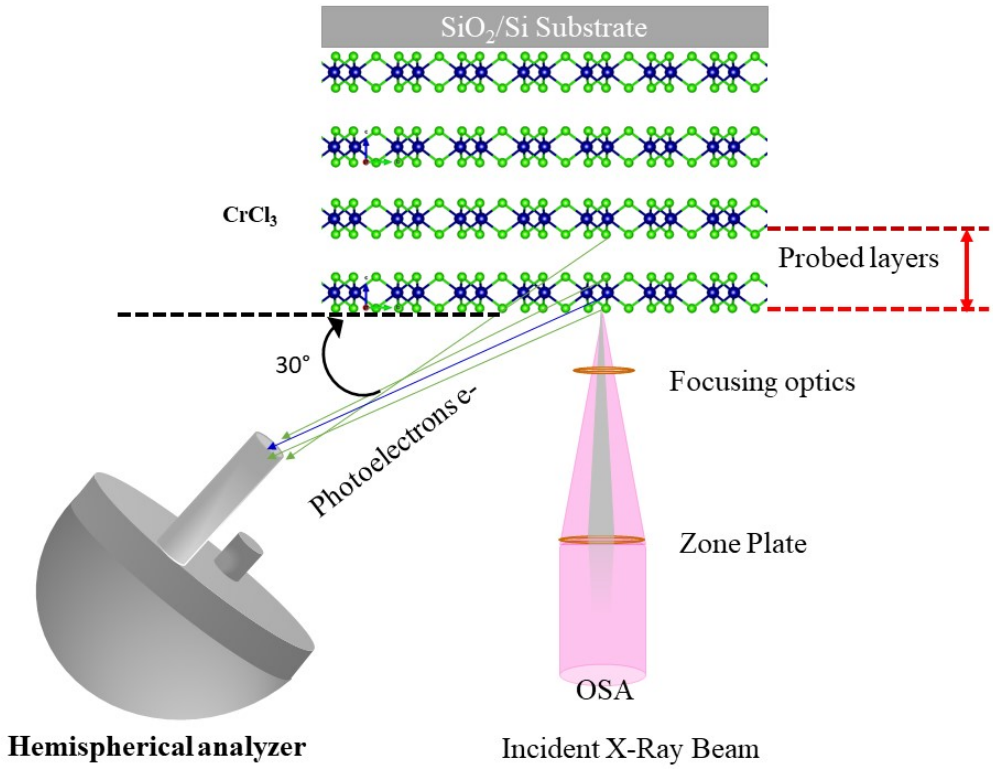

Figure 11: A schematic of SPEM experimental setup in the case of a few layer $CrCl_3$ flake.[27]. The lower part of the figure 11 was redrawn from reference [36].

References

1. Huang, B.; Clark, G.; Navarro-Moratalla, E.; Klein, D. R.; Cheng, R.; Seyler, K. L.; Zhong, D.; Schmidgall, E.; McGuire, M. A.; Cobden, D. H. et al. *Nature* **2017**, *546* (7657), 270–273. doi:10.1038/nature22391.

2. Kazim, S.; Ali, M.; Palleschi, S.; D'Olimpio, G.; Mastrippolito, D.; Politano, A.; Gunnella, R.; Di Cicco, A.; Renzelli, M.; Moccia, G. et al. *Nanotechnology* **2020**, *31*, 395706. doi:10.1088/1361-6528/ab7de6.

3. Wang, J.; Ahmadi, Z.; Lujan, D.; Choe, J.; Taniguchi, T.; Watanabe, K.; Li, X.; Shield, J. E.; Hong, X. *Advanced Science* **2023**, *10* (3), 2203548. doi:10.1002/advs.202203548.

4. Rhodes, D.; Chae, S. H.; Ribeiro-Palau, R.; Hone, J. *Nat. Mat.* **2019**, *18* (6), 541–549. doi:10.1038/s41563-019-0366-8.

5. Kundu, A. K.; Liu, Y.; Petrovic, C.; Valla, T. *Scientific Reports* **2020**, *10* (1), 15602. doi:10.1038/s41598-020-72487-5.

6. Biesinger, M.; Brown, C.; Mycroft, J.; Davidson, R.; McIntyre, N. *Surface and interface analysis: an international journal devoted to the development and application of techniques for the analysis of surfaces, interfaces and thin films* **2004**, *36* (12), 1550–1563. doi:10.1002/sia.1983.

7. Antoci, S.; Mihich, L. *Physical Review B* **1978**, *18*, 5768–5774. doi:10.1103/PhysRevB.18.5768.

8. Kazim, S.; Mastrippolito, D.; Moras, P.; Jugovac, M.; Klimczuk, T.; Ali, M.; Ottaviano, L.; Gunnella, R. *Physical Chemistry Chemical Physics* **2023**, *25*, 3806–3814. doi:10.1039/D2CP04586A.

9. Mastrippolito, D.; Wang, J.; Profeta, G.; Ottaviano, L. *Journal of Physics: Materials* **2022**, *5* (1), 014004. doi:10.1088/2515-7639/ac5dcd.

10. Mastrippolito, D.; Ottaviano, L.; Wang, J.; Yang, J.; Gao, F.; Ali, M.; D'Olimpio, G.; Politano, A.; Palleschi, S.; Kazim, S. et al. *Nanoscale Advances* **2021**, *3* (16), 4756–4766. doi: 10.1039/D1NA00401H.

11. Kazim, S.; Gunnella, R.; Zannotti, M.; Giovannetti, R.; Klimczuk, T.; Ottaviano, L. *Journal of Microscopy* **2021**, *283*, 145–150. doi:10.1111/jmi.13015.

12. Liu, L.; Zhai, K.; Nie, A.; Lv, W.; Yang, B.; Mu, C.; Xiang, J.; Wen, F.; Zhao, Z.; Zeng, Z. et al. *ACS Applied Nano Materials* **2019**, *2* (3), 1597–1603. doi:10.1021/acsanm.9b00058.

13. Kazim, S.; Sharma, A.; Yadav, S.; Gajar, B.; Joshi, L. M.; Mishra, M.; Gupta, G.; Husale, S.; Gupta, A.; Sahoo, S. et al. *Scientific reports* **2017**, *7* (1), 1–10. doi:10.1038/s41598-017-00976-1.

14. Banhart, F.; Kotakoski, J.; Krasheninnikov, A. V. *ACS nano* **2011**, *5* (1), 26–41. doi:10.1021/nn102598m.

15. Gao, Y.; Wang, J.; Li, Y.; Xia, M.; Li, Z.; Gao, F. *Physica Status Solidi (RRL)–Rapid Research Letters* **2018**, *12* (7), 1800105. doi:10.1002/pssr.201800105.

16. Zheng, Y. J.; Chen, Y.; Huang, Y. L.; Gogoi, P. K.; Li, M.-Y.; Li, L.-J.; Trevisanutto, P. E.; Wang, Q.; Pennycook, S. J.; Wee, A. T. S.; Quek, S. Y. *ACS Nano* **2019**, *13*, 6050–6059. doi: 10.1021/acsnano.9b02316.

17. Zhang, W.-B.; Qu, Q.; Zhu, P.; Lam, C.-H. *J. Mat. Chem. C* **2015**, *3* (48), 12457–12468. doi:10.1039/C5TC02840J.

18. Xie, D.; Yang, F.; Qiu, X.; Hu, Y.; Sun, Y.; He, S.; Wang, X. *J. Appl. Phys.* **2024**, *135*, 235105. doi:10.1063/5.0206006.

19. Haffad, S.; Benchallal, L.; Lamiri, L.; Boubenider, F.; Zitoune, H.; Kahouadji, B.; Samah, M. *Acta Physical Polonica A* **2018**, *133* (5), 1307. doi:10.12693/APhysPolA.133.1307.

20. Avsar, A.; Ciarrocchi, A.; Pizzochero, M.; Unuchek, D.; Yazyev, O. V.; Kis, A. *Nature nanotechnology* **2019**, *14* (7), 674–678. doi:10.1038/s41565-019-0467-1.

21. Liu, J.; Sun, Q.; Kawazoe, Y.; Jena, P. *Physical Chemistry Chemical Physics* **2016**, *18* (13), 8777–8784. doi:10.1039/C5CP04835D.

22. Pramanik, A.; Pandeya, R. P.; Ali, K.; Joshi, B.; Sarkar, I.; Moras, P.; Sheverdyaeva, P. M.; Kundu, A. K.; Carbone, C.; Thamizhavel, A. et al. *Physical Review B* **2020**, *101* (3), 035426. doi:10.1103/PhysRevB.101.035426.

23. Zeller, P.; Amati, M.; Sezen, H.; Scardamaglia, M.; Struzzi, C.; Bittencourt, C.; Lantz, G.; Hajlaoui, M.; Papalazarou, E.; Marino, M. et al. *physica status solidi (a)* **2018**, *215* (19), 1800308. doi:10.1002/pssa.201800308.

24. Parmar, R.; de Freitas Neto, D.; Kazim, S.; Rezvani, S.; Rosolen, J.; Gunnella, R.; Amati, M.; Gregoratti, L. *Journal of Alloys and Compounds* **2021**, *888*, 161483. doi:10.1016/j.jallcom.2021.161483.

25. Azizinia, M.; Salvato, M.; Castrucci, P.; Amati, M.; Gregoratti, L.; Parmar, R.; Rauf, M.; Gunnella, R. *APPLIED SURFACE SCIENCE* **2024**, *675*, 160899. doi:10.1016/j.apsusc.2024.160899.

26. Rezvani, S. J.; Abdi, Y.; Parmar, R.; Paparoni, F.; Antonini, S.; Gunnella, R.; Di Cicco, A.; Amati, M.; Gregoratti, L.; Mazaheri, A.; Hajibaba, S. *ACS APPLIED NANO MATERIALS* **2024**, *7* (11), 13712–13719. doi:10.1021/acsanm.4c02290.

27. S. Kazim, L. O. R. P. M. A. L. G., R. Gunnella Cl vacancy evaluation on the surface of $CrCl_3$ through ESCA microscopy. In *Società Italiana Luce di Sincrotrone Meeting 2021*; 2021.

28. Rohwerder M, T. F. *Electrochimica Acta* **2007**, *53* (7657), 290–299. doi:10.1016/j.electacta.2007.03.016.

29. Nonnenmacher, M.; o'Boyle, M.; Wickramasinghe, H. K. *Applied physics letters* **1991**, *58* (25), 2921–2923. doi:10.1063/1.105227.

30. Gunnella, R.; Rezvani, S. J.; Kazim, S.; Azizinia, M.; Ottaviano, L.; Mastrippolito, D.; Parmar, R.; Gregoratti, L.; Amati, M. A Detailed examination of layer-dependent photoemission spectra and surface potential of CrCl3. In *2023 IEEE Nanotechnology Materials and Devices Conference (NMDC)*; 2023; pp 173–173. doi:10.1109/NMDC57951.2023.10344256.

31. Poteryaev, A. I.; Ferrero, M.; Georges, A.; Parcollet, O. *Phys. Rev. B* **2008**, *78* (4), 045115. doi:10.1103/PhysRevB.78.045115.

32. Kim, J. H.; Lee, J.; Kim, J. H.; Hwang, C.; Lee, C.; Park, J. Y. *Applied Physics Letters* **2015**, *106* (25), 251606. doi:10.1063/1.4923202.

33. Neal, A. T.; Pachter, R.; Mou, S. *Applied Physics Letters* **2017**, *110* (19), 193103. doi:10.1063/1.4983092.

34. Kaushik, V.; Varandani, D.; Mehta, B. *The Journal of Physical Chemistry C* **2015**, *119* (34), 20136–20142.

35. DeJarld, M.; Campbell, P.; Friedman, A.; Currie, M.; Myers-Ward, R.; Boyd, A.; Rosenberg, S.; Pavunny, S.; Daniels, K.; Gaskill, D. *Scientific Report* **2018**, *8*, 16487. doi:10.1038/s41598-018-34595-1.

36. Gregoratti, L.; Al-Hada, M.; Amati, M.; Brescia, R.; Roccella, D.; Sezen, H.; Zeller, P. *Topics in Catalysis* **2018**, *61*, 1274–1282. doi:10.1007/s11244-018-0982-6.